American Mineralogist, Volume 75, pages 109–119, 1990

Structural distortions and vibrational modes in Mg_2SiO_4

Pui K. Lam, Rici Yu, Matthew W. Lee
Department of Physics and Astronomy, University of Hawaii at Manoa, 2505 Correa Road, Honolulu, Hawaii 96822, U.S.A.
Shiv K. Sharma
Hawaii Institute of Geophysics, University of Hawaii at Manoa, 2525 Correa Road, Honolulu, Hawaii 96822, U.S.A.

Abstract

A pair-potential model consisting of ionic interactions, core-core repulsions, and covalent interactions is used to simulate the lattice energy of forsterite (Mg_2SiO_4). The microscopic interactions responsible for the distortions of SiO_4 tetrahedra and the systematic variation of the high frequency modes of olivines are identified. The skewing of the tetrahedra is attributed to the forces on Si and oxygen ions caused by the Coulomb interactions with Mg ions. The observed trends of the high frequency ν_3- and ν_1-derived modes in olivines are related to variation in intertetrahedral O-O Coulomb interactions.

Introduction

Forsterite (Mg_2SiO_4, Fo) and fayalite (Fe_2SiO_4, Fa) form complete solid solutions known as olivines. The Mg-rich olivines are the most common minerals in the Earth's upper mantle; knowledge of the vibrational and structural properties of Fo is important for understanding a number of geophysical processes. Kieffer and Navrotsky (1985) stressed that a full understanding of the macroscopic behavior of minerals relies on a detailed knowledge of the microscopic interactions. At present, a first-principles quantum mechanical treatment of systems as complicated as Earth minerals is computationally difficult. Our aim is to model the microscopic interactions in terms of pairwise atomistic potentials, an approach that has been shown to be quite successful (Price and Parker, 1984; Price et al., 1987), and to use the model to study some chemical trends. We must emphasize that the pair-potential model is an empirical and approximate representation of the microscopic interactions; it is not unique and the interpretations are model dependent. However, if the model can account for a variety of properties and has a predictive capability, then it may be deemed useful.

Various pair-potential models have been proposed for forsterite and related silicates: a model with full ionic charge and Born-Mayer repulsion (Miyamoto and Takeda, 1980); a model with partial ionic charge, Born-Mayer repulsion, and rigid SiO_4 tetrahedra (Matsui and Bushing, 1984; Catti, 1981, 1982); and a model with partial ionic charge, Born-Mayer repulsion, and covalent interaction for Si-O (Price and Parker, 1984). A detailed comparison of these models was given by Price and Parker (1984). The models differ slightly on the expressions for the potentials and the way the parameters are obtained. The pair-potential parameters are usually obtained by fitting to one type of data (such as structural data); then the parameters are used to predict other data (such as elastic data). Although calculated macroscopic properties are presented in previous reports, there is often not enough discussion on the connection between the macroscopic properties and the microscopic interactions. In this paper, we discuss in detail the connection between the microscopic interactions and the macroscopic properties. As for the choice of pair-potential, we use a model proposed recently by Rao et al. (1987, 1988) as a starting point and modify the parameters to fit other experimental data such as the isotopic frequency shifts (Paques-Ledent and Tarte, 1973). The derived parameters do seem to make "physical or chemical" sense, and that is important for our present purpose. Our current computer code does not perform an automated search of the optimal pair-potential parameters, unlike programs such as WMIN (Bushing, 1981) and METAPOCS (Parker, 1983); our procedure is performed manually. In the process of adjusting the parameters, we have learned a great deal about how the microscopic parameters affect the macroscopic properties.

We will focus on certain experimental observations that are not well described by current models. For example, an isotopic experiment (Paques-Ledent and Tarte, 1973) indicates that the intense Raman (A_g) modes at 824 cm^{-1} (Ω_-) and 855 cm^{-1} (Ω_+) have a strong mixing of ν_1 and ν_3 characters, whereas the highest mode at 966 cm^{-1} (ω_3) has a nearly pure ν_3 character [the same notations for the frequencies were used by Piriou and McMillan (1983)]. For forsterite, the Ω_+ mode has more ν_1 character whereas the Ω_- mode has more ν_3 character. Experimental evidence also indicates a crossover in the ν_1-ν_3 mixing as Mg is replaced by a larger cation such as Ca (Handke, 1986; Piriou and McMillan, 1983); for example, the lower frequency mode, Ω_-, has more ν_1 character in γ-Ca_2SiO_4. So far, lattice-dynamics calculations have not reproduced the correct mixing or the crossover behavior (Oehler and Gunthard, 1969; Iishi, 1978; Price et al., 1987). Systematic variation in the Ω_-, Ω_+, and ω_3 frequencies also occur as a function of the size of the cation. Piriou and McMillan (1983) analyzed this trend with a simple coupling

0003–004X/90/0102–0109$02.00

TABLE 1. Lattice parameters and atomic coordinates of forsterite (*Pbnm*, Z = 4)

Atom	X	Y	Z
MgI	0.0000	0.0000	0.0000
	(0.0)	(0.0)	(0.0)
MgII	−0.0085	0.2774	0.2500
	(0.0)	(0.25)	(0.25)
Si	0.4262	0.0940	0.2500
	(0.375)	(0.0833)	(0.25)
O1	0.7657	0.0913	0.2500
	(0.75)	(0.0833)	(0.25)
O2	0.2785	−0.0526	0.2500
	(0.25)	(−0.0833)	(0.25)
O3, O4	0.2777	0.1628	0.0331
	(0.25)	(0.1667)	(0.0)

a = 4.7535 Å, b = 10.1943 Å, c = 5.9807 Å
(a = 4.8125 Å, b = 10.2089 Å, c = 5.8738 Å)

Note: The corresponding values in an ideal structure with the same unit-cell volume are given in parentheses.

model that accounted qualitatively and semiquantitatively for the variation of the high-frequency modes of olivines, but the physical origin of these systematic variations was not identified. Systematic variations in the bond lengths and bond angles of the SiO_4 tetrahedron are also functions of the size of the cation (Piriou and McMillan, 1983); the tetrahedron becomes more regular as the size of the cation becomes larger. This trend has not been explained in terms of microscopic forces.

Crystal structure and group symmetry

Forsterite (*Pbnm*, Z = 4) has an orthorhombic unit cell that contains four formula units of Mg_2SiO_4 (Hazen, 1976; Brown, 1980). The two cation sites are inequivalent; they are M_1 (a site) and M_2 (c site). The four oxygen sites are O_1 (c site), O_2 (c site), $O_3 = O_4$ (d site); Wyckoff site labels are given in parentheses (Hahn, 1983). The lattice parameters and the essential atomic coordinates (Hazen, 1976) are listed in Table 1. The corresponding values for an ideal olivine structure (with the same unit-cell volume) are given in parentheses. The other atomic coordinates inside the unit cell can be obtained from the symmetry operations listed in Table 2. We have translated the position of O_2 by a symmetry operation so that it is in the same tetrahedron as the other oxygens. Piriou and McMillan (1983) pointed out that Hazen's (1976) analysis for forsterite gave much too low a value for the Si-O_2 distance, 1.640 Å. We find that the atomic positions given by Hazen (1976) are similar to those of other refinements (Birle et al., 1968; Brown, 1980); the error was in Hazen's calculation of the distances. From Hazen's coordinates, we calculate the Si-O_2 distance to be 1.654 Å, which coincides with that of Birle et al. (1968).

The symmetry group for the vibrational modes at the zone center ($k = 0$) is isomorphic to the D_{2h} point group and can be factored into the following symmetries or irreducible representations (Oehler and Gunthard, 1969; Burns and Glazer, 1978):

$$\Gamma^{\text{total}} = 11A_g + 11B_{1g} + 7B_{2g} + 7B_{3g} + 10A_u + 10B_{1u} + 14B_{2u} + 14B_{3u}, \quad (1)$$

where three of them are purely translational modes, $B_{1u} + B_{2u} + B_{3u}$, the g modes are Raman active, A_u is spectroscopically inactive, and the rest of the u modes are infrared active.

We find two useful ways to visualize the crystal structure:

Linked SiO_4 tetrahedra. SiO_4 tetrahedra are linked together by Mg ions. The Mg-O Coulomb attraction pulls the isolated tetrahedra together whereas the intertetrahedral O-O repulsion (Born-Mayer) and the Mg-O repulsion (Born-Mayer) prevent them from collapsing. This picture brings out the importance of the Mg-O interaction in governing the bulk modulus. This picture is also useful for analyzing the vibrational modes. One can start with the modes of an isolated tetrahedron and examine how these modes change and how additional modes arise as the intertetrahedral O-O and Mg-O interactions are being included.

Oxygen-ion lattice. Starting with oxygen ions in a hexagonal–close-packed (hcp) structure, Si and Mg ions are added to some of the tetrahedral and octahedral holes, respectively, in the hcp structure. This picture is useful for visualizing the driving forces for the structural distortion from the ideal structure.

Theoretical models

Calculational method

The lattice energy is represented by a sum of pair-wise potentials. The force on an atom is obtained by calculating the derivative of the lattice energy with respect to the atomic displacement. The phonon frequencies and the corresponding atomic displacements are obtained by diagonalizing the dynamical matrix. The expression for the dynamical matrix is given in well-known texts such as Born and Huang (1954) and Maradudin (1974). Our pair-potential model includes the long-range Coulomb interactions; therefore, an Ewald-summation technique is used to ensure good convergence of the results (Maradudin, 1974). A force-constant model is also used to study the dependence of the phonon frequency on the various force

TABLE 2. Symmetry operations for forsterite

R_k:	E	$C_2(Z)$	$C_2(Y)$	$C_2(X)$	i	$\sigma(Z)$	$\sigma(Y)$	$\sigma(X)$
		1	1 1 1	1 1		1	1 1 1	1 1
t_{τ_k}:	0	(0, 0, —)	(—, —, —)	(—, —, 0)	0	(0, 0, —)	(—, —, —)	(—, —, 0)
		2	2 2 2	2 2		2	2 2 2	2 2

constants. We have tested our computer codes by reproducing the previous force-constant results of forsterite by Oehler and Gunthard (1969) and reproducing the pair-potential results of NaCl by Kellermann (1940).

Pair-potential model

The forms for the pair potentials used in this study are similar to those used by Rao et al. (1987, 1988) but with some modifications. We start with an ionic model of the crystal. The interaction between any two ions is given by a Coulomb interaction term and a Born-Mayer core-core repulsion term:

$$V_i(r) = \frac{Z_i Z_j e^2}{r} + a \exp[-br/(R_i + R_j)], \qquad (2)$$

where Z_i and Z_j are the ionic charges of the ith and jth ions, r is the distance between them, R_i and R_j are the radii parameters, and a and b are the Born-Mayer parameters. The parameters Z_i, Z_j, R_i, R_j, a, and b are adjusted to fit the observed frequencies and structural properties. Note that the radii parameters are adjustable parameters; their values need not coincide with the ionic radii used in structural studies (Pauling, 1960). In fact, the values of the radii parameter depend on the value of b; one can simultaneously rescale all the radii and the value of b without changing the potential in Equation 1. Rao et al. (1987, 1988) used the above ionic description for the "nonbonded" ions only. In principle, the Coulomb interaction should be present for both nonbonded and bonded ions. Furthermore, Rao et al. increased the Born-Mayer repulsion for the intratetrahedral O-O by a factor of 55 and compensated the effect partly by including a Van der Waals attraction term, $-W/r^6$. Price et al. (1987) also enhanced the O-O repulsion and included a Van der Waals term. In our study, we find that the dominant contribution to the O-O force constant is the O-O Coulomb repulsion rather than the Born-Mayer repulsion. We did not find it necessary to use different Born-Mayer parameters for the intratetrahedral and intertetrahedral O-O interaction. We also did not include the Van der Waals term.

For the Si-O bond, we include an *additional* term that describes the covalent bond:

$$V_c(r) = -d \exp[-c(r - r_o)^2/r], \qquad (3)$$

where d, c, and r_o are adjustable parameters. This is an additional contribution to the interaction between Si and O. In the work of Rao et al. (1987, 1988), the Si-O interaction contained only the covalent term. Price and Parker (1984) modeled the Si-O covalent interaction by a Morse potential, but later they showed that the parameters obtained by fitting to the structural data were not able to describe the vibrational modes correctly (Price et al., 1987). So, they abandoned the Morse potential and used a "bond-bending" potential, which is a three-body potential. The fact that we are able to reproduce the vibrational frequencies with a pair-wise potential for the Si-O covalent interaction suggests that a Morse potential could also do the job provided the parameters are adjusted.

The parameters assigned by Rao et al. (1987, 1988) gave too large a frequency for the high-frequency modes; their calculated phonon density of states peaked around $\simeq 1100$ cm^{-1}. We have retained most of Rao et al.'s parameters but have modified some of them as necessary. The set of pair-potential parameters are chosen to give (1) satisfactory fit to the measured phonon frequency; (2) minimal forces on the atoms; and (3) satisfactory agreement with the isotopic frequency-shift data. The potential parameters used in this work are listed in Table 3. We use the same ionic charges and radii as assigned by Rao et al. (1988). The slightly different charges and radii among the oxygens and among the magnesiums reflect the inequivalency of these sites. Rao et al. (1988) assigned $a = 1882$ and $b = 12.364$ for the Born-Mayer parameters. In their 1987 article, Rao et al. assigned $b = 8.5$, but they scaled the radii by the same factor, so the results are the same. We also use $b = 12.364$, but we change the value of a for the Si-O and the O-O interactions. We find it necessary to have a Born-Mayer repulsion term for Si-O, but this term is small ($a = \frac{1}{2} \times 1882$) because part of the repulsion is already provided by the positive curvature of the covalent term. We find that in order to obtain satisfactory agreement with the isotopic shift experiment (especially the correct mixing of ν_1 and ν_3 for the high-frequency A_g modes), we need a large Born-Mayer parameter for the O-O interaction ($a = 3.5 \times 1882$). Price et al. (1987) also assigned the largest Born-Mayer parameter for the O-O interaction. We have given the Born-Mayer parameters in four and five significant figures for the sake of direct comparison with Rao et al.'s work. Actually, a change of a couple percent in the parameters would not alter the overall quality of the fit to the frequencies; root-mean-square error changes from 27 cm^{-1} to 30 cm^{-1}.

Force-constant model

We want to identify the connection between the frequency modes and the dominant interactions, and so we consider nearest-neighbor interactions only: Mg-Mg, Mg-Si, Mg-O, Si-O, and O-O (we also use the ideal structure). The force-constant parameters are adjusted to give the best overall fit to the experimental Raman frequencies and infrared frequencies (Iishi, 1978). The force constants (Table 4) are compared with those from Oehler and Gunthard (1969) and from Iishi (the short-range model, SR1, 1978). Oehler and Gunthard used the same model, and so a direct comparison can be made between their force constants and ours. However, Iishi used a slightly different model. Oehler and Gunthard fitted their force constants to their infrared data only. They obtained an unusually large Mg-Mg force constant. As pointed out by Paques-Ledent and Tarte (1973), the vibrational mode assignments of Oehler and Gunthard are inconsistent with the observed isotopic shifts in the IR and Raman spectra of Mg_2SiO_4. For example, Oehler and Gunthard concluded

TABLE 3. Pair-potential parameters

Atom:	M_1	M_2	Si	O_1	O_2	O_3	O_4
			Effective charges and radii parameters				
Charges*	1.60	1.60	1.0	−1.2	−1.0	−1.10	−1.10
Radii (Å)	1.68	1.73	1.0	1.55	1.45	1.50	1.50
	a (eV)		b (Å^{-1})	c (Å^{-1})	d (eV)		r_o (Å)
			Short-range pair-potential parameters†				
M-M	1882		12.364	0	0		0
Si-M	1882		12.364	0	0		0
Si-Si	1882		12.364	0	0		0
O-M	1882		12.364	0	0		0
O-Si	941		12.364	5.25	3.7		1.635
O-O	6587		12.364	0	0		0

* In units of proton charge.
† M stands for both M_1 and M_2.

ed that an infrared band at around 880 cm^{-1} is dominated by the Mg-Mg and Mg-O force constants. This is in contradiction with the isotope-shift results of Paques-Ledent and Tarte. Oehler and Gunthard also obtained an unusually large Si-O force constant (4.63 mdyn/Å) for forsterite. This value can be traced to a probable error in two of their measured IR frequencies (see the two frequencies indicated by double asterisks in Table 5). Their Si-O force constant for Ca_2SiO_4 is 3.42 mdyn/Å, which is much closer to our value (3.76 mdyn/Å) and to that of Iishi for forsterite (3.468 mdyn/Å).

RESULTS AND DISCUSSION

Distortion of the SiO_4 tetrahedron in the olivines

Various models have been proposed to explain the distortions. For example, Baur (1972) proposed a geometric model where the distortions are explained in terms of misfitted polyhedra (the tetrahedral and the octahedral volumes do not have the ideal ratio). McLarnan et al. (1979) used semiempirical molecular orbital calculations to study the distortion in the bond angles and the intratetrahedral O-O distances but did not study the distortion in the Si-O bond distances. These models are either so simple that the underlying forces are not considered or are so complicated that the interpretations are difficult. The advantage of the pair-potential approach is that one can interpret the pair-potential in terms of the microscopic interactions and yet avoid the complexity of quantum treatment. We use the idealized olivine structure as the reference and investigate the microscopic forces that are responsible for distorting the ideal structure to the experimental observed structure. There are various aspects of the distortion in going from the ideal structure to the real structure. For example, the lattice parameters are distorted from the ideal ratio (a:b:c = 1:3/$\sqrt{2}$:$\sqrt{(3/2)}$ (see Table 1); the tetrahedral volume is contracted compared to the octahedral volume; the SiO_4 tetrahedra are skewed. Our focus will be on the distortion of the SiO_4 tetrahedron.

TABLE 4. Force constants (mdyn/Å) for forsterite

	1	2	3
F(Mg-Mg)	0.22	1.94	—
F(Mg-Si)	0.53	0.30	0.151
F(Mg-O)	0.25	0.30	0.456
F(Si-O)	3.76	4.63	3.468
F(O-O)	0.44	0.34	0.654–1.09*
			0.231†

Note: In the present work (column 1; 22 °C) and the work of Oehler and Gunthard (1969; column 2; −175 and −235 °C), the force constants are for the ideal structure; in Iishi's work (1978; column 3), the force constants are for the experimentally determined structure.
* Intratetrahedral O–O.
† Intertetrahedral O–O.

If we start with the oxygen ions in a hcp lattice, there are no forces on the oxygens because of lattice symmetry. After Si is added to the tetrahedral holes, the "local" environment of the four oxygens of a tetrahedron remains approximately equivalent. The covalent interaction between Si and oxygen causes the contraction of the Si-O distances without skewing the tetrahedral symmetry. The Si-O distance in the ideal structure is 1.805 Å (computed from the atomic position given in Table 1) as compared to 1.615–1.651 Å in the real forsterite structure. However, after the magnesiums are added to some of the octahedral holes, the local environment of O_1 differs greatly from that of the other oxygens (see Fig. 1). The O_1 and its three nearest neighbor magnesiums are noncoplanar whereas the other oxygens form a nearly planar arrangement with their three nearest-neighbor magnesiums. Since only some of the octhedral holes are filled, there are unbalanced forces on the tetrahedra. We find that the dominant forces for the skewing of the tetrahedron are forces on Si and oxygen that come from the Mg-O and the Mg-Si Coulomb interactions; the Born-Mayer repulsion serves to limit the amount of distortion. The net forces on the atoms (not including the covalent force) are shown in Figure 2. Since the Coulomb interaction is spatially long range, the summation of the forces are performed with an Ewald-type of summation technique. However, the direction of some of the forces can be accounted for by considering only the nearest-neighbor interactions. We

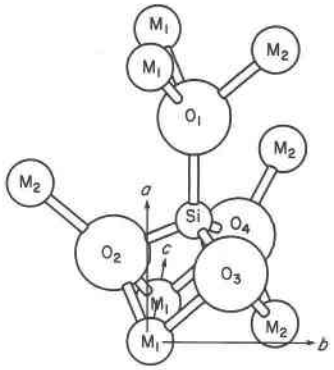

Fig. 1. Local environment of a SiO_4 tetrahedron in forsterite. The Si is closer to the three cations at the base than to the three on the top.

will discuss the dominant forces on each atom with specific reference to Figure 1:

Force on Si. There is a net force on the Si that is directed toward O_1. The largest contribution to this force comes from the Coulomb repulsion between Si and the three basal magnesiums (the Si-Mg distance is 2.48 Å in the ideal structure; see Fig. 1). The three magnesiums on the top of the tetrahedron are farther from the Si (the Si-Mg distance is 3.64 Å in the ideal structure); therefore, the Coulomb repulsion from these three magnesiums does not cancel that from the basal magnesiums. This force on Si is responsible for making the Si-O_1 distance shorter than the other Si-O distances. The Coulomb interaction between Si and all the oxygens causes a small force on the Si in the negative *a* direction, and the Si-Si Coulomb repulsion causes a small lateral force in the positive *b* direction.

Force on O_1. The net force on O_1 is nearly zero. The Coulomb attraction and the Born-Mayer repulsion from the three magnesiums on the top balance almost exactly those from the Si underneath. This is consistent with the O_1 ionic position having the least amount of distortion (Table 1). Since there is also no net force on M_1 because of inversion symmetry, the M_1-O_1 distance (2.084 Å) is the same in both the real forsterite structure and the ideal structure.

Force on O_2. Both the covalent and the Si-O Coulomb attraction exert a force on O_2 that is directed toward the central Si. (Actually, the total Si-O Coulomb force is not exactly directed toward the central Si because of the presence of other silicons.) The Mg-O Coulomb attraction exerts a small downward force on O_2. The direction of this downward force can be explained by considering the contribution from the three nearest magnesiums. The combination of the central and downward force creates a bending force on O_2 with respect to the central Si (see Fig. 2). This bending force is consistent with the observed distortion.

Force on O_3 (O_4). The forces on O_3 are similar to those on O_2, i.e., the combined central and downward force creates a bending force.

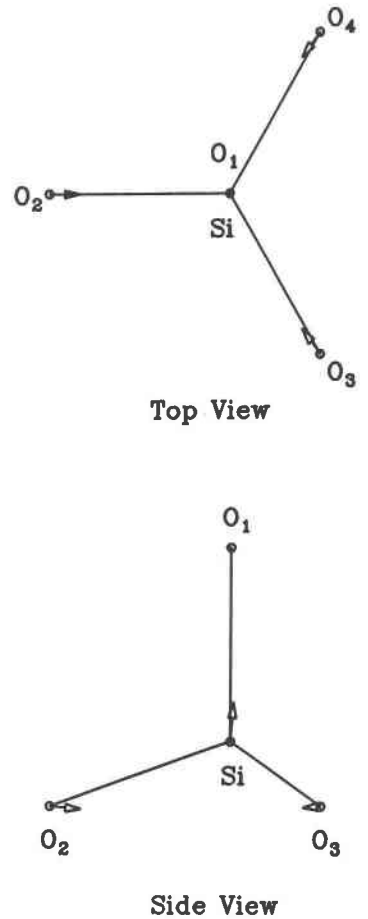

Fig. 2. Forces on the ideal SiO_4 tetrahedron. Si-O covalent force is not included. The force on O_1 is nearly zero.

The observed trend is that as the cation size increases, the Si-O tetrahedron becomes more regular. This trend is consistent with our analysis of the forces above. As the cation size increases, the Si-M distance and O-M distance increase, hence reducing the Coulomb interactions that cause the skewing of the tetrahedron. There is, however, a small counter effect. Generally, larger cations are more electro-positive. The ionic charge of a large cation would be more positive, and the oxygen ion would be more negative, thus increasing the Coulomb interaction. However, the increase in the ionic charge is expected to be only a few percent, whereas the Si-M and O-M distances change by 10% from Mg_2SiO_4 to γ-Ca_2SiO_4. Since the Coulomb force is proportional to r^{-2}, a 10% change in the distance causes ~20% change in the force.

Comparison between calculated and measured frequencies

Polarized Raman spectra of an oriented single crystal of forsterite were recorded at room temperature with a SPEX 1402 double monochromator. Data acquisition was controlled by a SPEX Datamate computer. The crystal was excited with the 488.0-nm line (500 mW) of an Ar^+ ion laser, and a spectral slit width of 2 cm^{-1} was used. The

TABLE 5. Calculated (pair-potential model) and measured phonon frequencies at $k = 0$ and their isotopic shifts

Experimental frequencies (cm^{-1})*				Theory*	Calculated isotopic shifts			Experimental isotopic shifts	
Ref. 1	Ref. 2	Ref. 3	Ref. 4	Ref. 1	^{30}Si	^{26}Mg	^{18}O	^{30}Si	^{26}Mg
Raman mode A_g									
183	—	183	—	172	1	2	5	—	—
227	—	227	—	209	3	1	6	—	—
305	—	305	—	293	1	4	10	—	—
330	—	329	—	305	0	0	14	—	—
340	—	340	—	372	0	10	5	—	—
424	—	424	—	421	0	4	15	—	—
546	—	546	—	519	2	0	26	—	—
608	—	609	—	577	4	0	25	—	—
824	—	826	823	844	6	0	43	5.5	—
856	—	856	856	863	4	0	36	3.5	—
965	—	966	959	956	11	0	33	8	—
Raman mode B_{1g}									
189	—	192	—	213	3	1	6	—	—
220	—	224	—	251	3	2	7	—	—
260	—	260	—	314	1	4	11	—	—
319	—	318	—	351	0	3	16	—	—
418	—	418	—	359	2	5	7	—	—
434	—	434	—	423	0	3	17	—	—
583	—	583	—	607	3	1	29	—	—
632	—	632	—	667	2	7	23	—	—
839	—	839	—	852	9	0	35	—	—
864	—	866	—	884	2	1	44	—	—
976	—	976	—	965	10	0	35	—	—
Raman mode B_{2g}									
142	—	142	—	150	1	2	4	—	—
243	—	244	—	251	1	0	13	—	—
303	—	324	—	329	2	5	9	—	—
364	—	368	—	341	0	0	17	—	—
439	—	441	—	449	0	2	22	—	—
586	—	588	—	595	2	0	30	—	—
881	—	884	—	877	10	0	31	—	—
Raman mode B_{3g}									
227	—	226	—	197	2	1	6	—	—
272	—	272	—	285	1	0	14	—	—
316	—	318	—	317	0	3	14	—	—
374	—	376	—	390	1	1	21	—	—
411	—	412	—	409	0	6	12	—	—
592	—	595	—	603	1	3	27	—	—
919	—	922	919	887	11	0	30	7	—
Infrared mode B_{1u}									
—	201	201	—	190	0	4	4	—	—
—	201	224	—	273	0	8	2	—	—
—	276	274	277	293	0	7	5	0.0	9.5
—	319	296	—	325	0	3	13	—	—
—	408	365	364	364	3	6	6	1.5	4.5
—	475	423	425.5	424	0	4	17	0.0	5.5
—	507	483	482	466	0	3	21	2.0	2.0
—	613	502	—	488	0	3	21	—	—
—	960	885	885	877	10	0	31	15.5	1.0
Infrared model B_{2u}									
—	144	144	—	133	1	1	4	—	—
—	201	224	—	295	1	8	2	—	—
—	276	280	—	304	2	6	4	—	—
—	301	294	—	365	0	4	16	—	—
—	361	352	—	418	2	8	15	—	—
—	421	400	—	425	1	3	8	—	—
—	507	421	415	458	1	9	11	3.0	10.0
—	540	465	466.5	483	0	9	10	3.0	11.0
—	613	510	—	543	2	6	17	—	—
—	837**	537	—	585	3	5	17	—	—
—	880	838	842	846	4	0	43	1.5	0.5
—	993	882	—	878	5	0	37	—	—
—	993	987	—	958	11	0	33	—	—

TABLE 5—*Continued*

Experimental frequencies (cm^{-1})*				Theory*	Calculated isotopic shifts			Experimental isotopic shifts	
Ref. 1	Ref. 2	Ref. 3	Ref. 4	Ref. 1	^{30}Si	^{26}Mg	^{18}O	^{30}Si	^{26}Mg
Infrared model B_{3u}									
—	201	201	—	214	2	2	5	—	—
—	224	224	—	261	1	5	5	—	—
—	276	274	—	300	0	7	6	—	—
—	295	293	—	323	2	6	4	—	—
—	381	320	—	391	1	9	11	—	—
—	421	378	384	401	0	3	12	0.0	2.0
—	462	403	—	466	1	5	17	—	—
—	475	498	—	526	0	10	16	—	—
—	613	562	601	538	4	2	17	2.0	1.5
—	837**	601	—	583	0	10	13	—	—
—	880	838	—	844	0	1	47	—	—
—	993	957	961.5	923	10	1	33	11.0	0.5
—	993	980	1001	955	11	0	33	1.0	3.0
Inactive model A_u									
—	—	—	—	117	1	2	3	—	—
—	—	—	—	161	1	2	4	—	—
—	—	—	—	225	0	5	4	—	—
—	—	—	—	286	0	4	10	—	—
—	—	—	—	347	2	4	9	—	—
—	—	—	—	376	0	4	15	—	—
—	—	—	—	437	0	10	8	—	—
—	—	—	—	469	1	6	15	—	—
—	—	—	—	511	0	4	20	—	—
—	—	—	—	885	10	0	31	—	—

* References are (1) this paper, (2) Oehler and Gunthard (1969), (3) Iishi (1978), and (4) Paques-Ledent and Tarte (1973). The measured frequencies from the unpolarized infrared and Raman results of Paques-Ledent and Tarte are tentatively assigned.
** These two frequencies from Oehler and Gunthard (1969) are probably incorrect.

scattered light was collected at 90° with respect to the excitation beam. Our Raman frequencies agree very well with those obtained by Iishi (1978), but differ from those obtained by Servoin and Piriou (1973), especially in the low-frequency region of the B_{1g}, B_{2g}, and B_{3g} modes.

The comparison between experimental and calculated phonon frequency from the pair-potential model is shown in Table 5. The overall fit to the measured frequencies is quite good; the root-mean-square deviation is $\simeq 27$ cm^{-1}. The isotopic shift is one convenient way to reveal the atomic motion of the modes. The calculated isotopic shifts corresponding to $^{28}Si \rightarrow {}^{30}Si$, $^{24}Mg \rightarrow {}^{26}Mg$, and $^{16}O \rightarrow {}^{18}O$ are also shown in Table 5. Since the A_u modes are spectroscopically inactive, these modes were not available as input to our fitting of the pair-potential parameters. It is interesting to note that our calculated A_u modes are very close to those of Price et al. (1987) except for the lowest and highest frequencies.

Before we discuss the systematic trend of the high-frequency modes in the olivines, we must understand the atomic motions of each mode and establish a relationship between the frequency modes and the underlying force constants (interactions). We find from the phonon eigenvector analysis that the highest A_g mode, ω_3 (966 cm^{-1}), is predominantly Si-O_1 stretch, the Ω_+ (855 cm^{-1}) mode is predominantly Si-O_3(O_4) stretch, and the Ω_- (824 cm^{-1}) mode is predominantly Si-O_2 stretch. This is consistent with the fact that Si-O_1 is the shortest bond and Si-O_2 is the longest. For simplicity, we had used only one value for the Si-O covalent term ($d = 3.7$). This does not mean that the force constants for all the Si-O bonds are the same because the Si-O Born-Mayer term and the Si-O Coulomb term depend on distance. However, the Born-Mayer and the Coulomb term are not enough to account for the variation in force constant for the different Si-O bonds. As we can see from Table 5, the calculated Ω_- (844 cm^{-1}) is too high whereas the calculated ω_3 (956 cm^{-1}) is too low. We can bring the calculated frequencies into better agreement with experiment by adjusting the Si-O covalent term individually for Si-O_1, Si-O_2, and Si-O_3. If we choose $d = 3.8$ for Si-O_1 (bond distance = 1.615 Å), $d = 3.6$ for Si-O_3 (bond distance = 1.635 Å), and $d =$

TABLE 6. Effect of various force constants on the frequency distribution

	Isolated SiO_4		Forsterite	
	F(Si-O)	F(Si-O) + intratetrahedral F(O-O)	F(Si-O) + all F(O-O)	F(Si-O) + F(O-O) + F(Mg-O)
ν_3	837	860	875–915	885–920
ν_1	631	765	815–840	825–850
ν_4	0.15	234		
$\nu_4 + \nu_2$			400–575	440–600
ν_2	0.25	216		

Note: Frequencies are in units of cm^{-1}. The force constants are listed in Table 4.

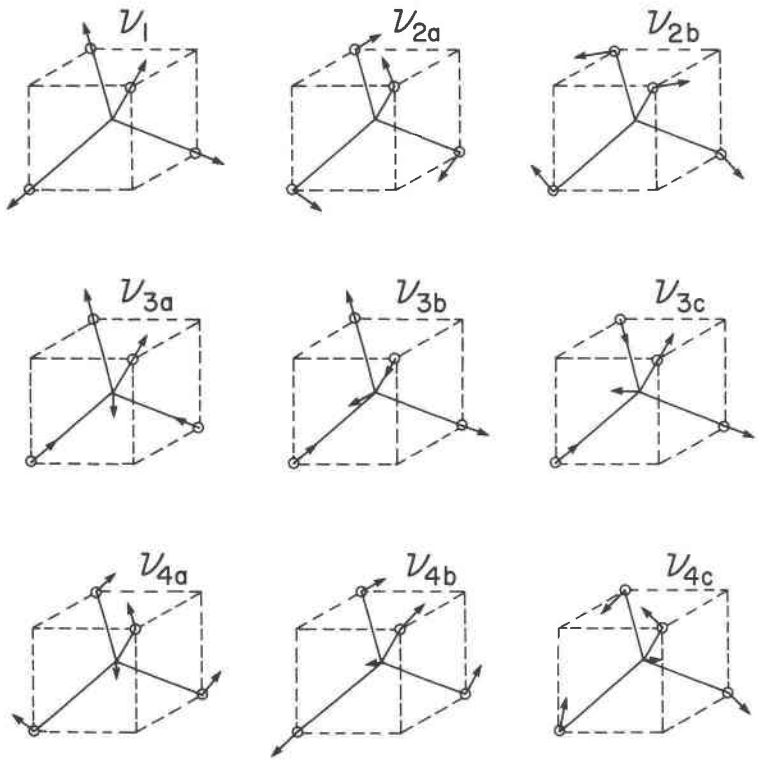

Fig. 3. Symmetry modes of an isolated SiO_4 tetrahedron.

3.5 for Si-O_2 (bond distance = 1.654 Å), we obtain $\Omega_- = 828$ cm^{-1}, $\Omega_+ = 858$ cm^{-1}, and $\omega_3 = 960$ cm^{-1}, in better agreement with experiment.

Dependence of vibrational modes on the individual force constants

We analyze the vibrational modes of forsterite in terms of interacting SiO_4 tetrahedra. We use the force-constant model for this study because the interactions can be controlled individually. The result is summarized in Table 6 and is discussed below.

An isolated SiO_4 tetrahedron. There are four types of symmetry modes: ν_3 (3), ν_1, ν_4 (3), and ν_2 (2), the degeneracy is indicated in parenthesis. The motions of these modes are shown in Figure 3 and are discussed below.

The ν_3 modes are the antisymmetric stretching modes of Si-O. These modes are most sensitive to the Si-O force constant and moderately sensitive to the O-O force constant.

The ν_1 mode is the symmetric stretching mode of Si-O. The Si atom is stationary. This mode is sensitive to both the Si-O and O-O force constants.

The ν_4 modes are the antisymmetric bending modes of oxygens. To first order, the Si-O bond distance does not change; hence these modes are only slightly sensitive to the Si-O force constant, but they are very sensitive to the O-O force constant.

The ν_2 modes are the symmetric bending modes of oxygens. The Si atom is stationary. These modes are sensitive to the O-O force constant.

When only the Si-O force constant is used, the ν_3 (antisymmetric stretch) frequency is always higher than the

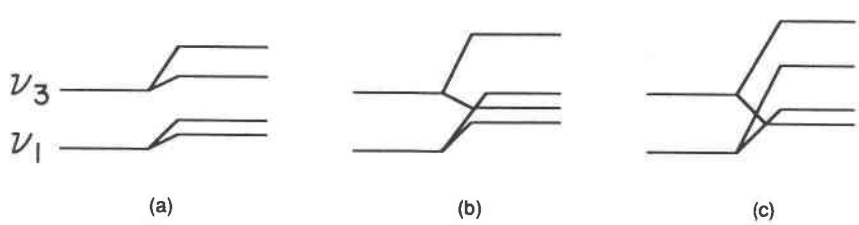

Fig. 4. A diagram showing qualitatively the amount of ν_1-ν_3 mixing and the ordering of the ν_1- and ν_3-derived modes in olivines as a function of the intertetrahedral O-O force constant, which increases from plot a to plot b to plot c.

ν_1 (symmetric stretch) frequency (first column in Table 6). The difference in the ν_3 and ν_1 frequencies is proportional to the Si-O force constant. When the intratetrahedral O-O force constant is included (Table 6, column 2), the ν_1 frequency increases more than the ν_3 frequency. In principle, a sufficiently large intratetrahedral O-O force constant can cause the order of the ν_3 and ν_1 frequencies to be reversed. However, the intratetrahedral O-O force constant is normally not large enough to cause such reversal in an isolated SiO_4 tetrahedron. But, when the tetrahedra are placed in a crystal, there are additional O-O force constants from the intertetrahedral interaction. If the intertetrahedral O-O force constant is large enough, it could push the ν_1-derived modes higher than some of the ν_3-derived modes (Fig. 4c). We believe that it is the variation in the intertetrahedral O-O force constant among the olivines that causes the crossover behavior in the ν_1-ν_3 mixing of the high-frequency A_g modes. A more detailed discussion is given in the section on Relationships between the High-Frequency Modes and Structure of Olivines.

Forsterite as interacting tetrahedra. The interactions between tetrahedra produce perturbations on the eigenmodes of an isolated tetrahedron. Three effects can take place: the frequencies of the modes increase because of additional force constants, the degeneracies of the modes are lifted, and the different symmetries of the unperturbed modes (ν_3, ν_1, ν_4, and ν_2) are mixed. We discuss the effect of each intertetrahedral interaction individually.

The ν_4- and ν_2-derived modes are the most sensitive to the inclusion of the intertetrahedral O-O force constants (Table 6, column 3); the frequencies are nearly doubled. This doubling of the frequency is caused by the fact that each oxygen is interacting with 12 nearest-neighbor oxygens (the oxygens form a hcp structure) as compared to 3 neighbors in the isolated tetrahedron. The force constant for these modes increases by a factor of 4, and hence the frequencies increase by a factor of 2. Since the unperturbed ν_4 and ν_2 modes are very close in frequency, the eigenmodes in the crystal are a strong mixture of these two symmetry modes.

The intertetrahedral O-O force constants increase the frequencies of the ν_1-derived modes more than those of the ν_3-derived modes. However, the spread of the ν_3 modes is larger than that of the ν_1 modes. The spread in the ν_3 modes is caused mainly by the lifting of degeneracy within a tetrahedron whereas the spread of the ν_1 modes is caused by mixing of ν_1 modes from different tetrahedra. There is practically no mixing between the ν_3 and ν_1 modes with our force-constant model because we have chosen a Si-O force constant large enough that separation between the unperturbed ν_3 and ν_1 frequencies is large and an intertetrahedral O-O force constant small enough that there is no significant mixing. The fact that our chosen Si-O force constant is too large is related to our using only one Si-O force constant for all the Si-O bonds. In the real forsterite structure, the Si-O bond distances within a tetrahedron are different. The $Si\text{-}O_1$ bond is the shortest, and the $Si\text{-}O_2$ bond is the longest. The longest Si-O bond ($Si\text{-}O_2$) should have a smaller force constant, thus bringing some of the ν_3-derived modes closer in frequency to the ν_1-derived modes. By using different force constants for the different Si-O bonds, we are able to obtain the proper mixing of ν_3 and ν_1 modes. We believe that this could be the reason why previous lattice-dynamics calculations did not obtain the correct ν_1-ν_3 mixing; the Si-O force constants used were too large for the $Si\text{-}O_2$ bond.

The ν_3- and ν_1-derived modes (Table 6, column 4) are increased further by the Mg-O interaction but only slightly ($\simeq$10 cm^{-1}) whereas the ν_4- and ν_2-derived modes are increased a little bit more ($\simeq$30 cm^{-1}).

The force constants of the Mg-Si and Mg-Mg interactions have very small effects on the vibrational modes.

Isotopic frequency shifts and mode assignments

Paques-Ledent and Tarte (1973) had performed isotopic substitution experiments on forsterite. They replaced ^{28}Si by ^{30}Si and ^{24}Mg by ^{26}Mg and measured the frequency shifts. Previous lattice-dynamics calculations (Iishi, 1978; Price et al., 1987) have assigned the following characters to the three highest A_g modes: 965 cm^{-1} (ν_3), 856 cm^{-1} (ν_3), and 824 cm^{-1} (ν_1). However, Paques-Ledent and Tarte found significant mixing of ν_3 and ν_1 characters for the 856 cm^{-1} and 824 cm^{-1} modes. The possibility of the 856 cm^{-1} mode having a strong ν_1 character has also been suggested by Piriou and McMillan (1983). The isotopic experimental result places further constraints on the potential parameters because a proper ratio of Si-O and O-O force constants is needed to reproduce the correct mixing of ν_3 and ν_1 characters. We have calculated the isotopic frequency shifts using the pair-potential model and compared our results with the isotopic exchange results of Paques-Ledent and Tarte (see Table 5). The masses for Si and Mg are computed according to the percentage of isotopic species in Paques-Ledent and Tarte's experiment. Since their data were not polarized measurements, we first matched their experimental frequency with the polarized measurement (Iishi, 1978) and then compared the calculated isotopic shift with the experimental shift. The agreement for the Raman mode is very good. Since Paques-Ledent and Tarte's infrared frequencies are quite different from those of Iishi (1978), there might be errors in matching up the frequencies. Furthermore, Piriou and McMillan (1983) had suggested that some of the infrared modes may be leakage from other longitudinal optical (LO) modes. We have not taken that into account.

From a rough estimate, a pure ν_3-derived mode of forsterite would have an isotopic shift of about 12 cm^{-1}, when ^{28}Si is replaced by ^{30}Si. A pure ν_1-derived mode has zero frequency shift for Si-isotope substitution. According to our calculated isotopic shift, the 965 cm^{-1} mode is almost entirely ν_3-derived. The 865 cm^{-1} and the 825 cm^{-1} modes are very close in frequency; therefore there is a strong ν_1-ν_3 mixing. The 865 cm^{-1} mode can be as-

signed approximately as 40% ν_3 and 60% ν_1, and the 825 cm^{-1} mode as 60% ν_3 and 40% ν_1.

Relationship between the high-frequency modes and structure of olivines

There is a systematic decrease of the high-frequency modes of olivines as the size of the cation increases (e.g., Piriou and McMillan, 1983). From Mg_2SiO_4 to γ-Ca_2SiO_4, the highest mode, ω_3, decreases by 40 cm^{-1}, the next highest mode, Ω_+, decreases by 17 cm^{-1}, and the third-highest mode, Ω_-, decreases by 11 cm^{-1} (Piriou and McMillan, 1983). From isotopic experiment and relative Raman intensities, it is concluded that there is significant ν_1-ν_3 mixing in Ω_- and Ω_+. In Mg_2SiO_4, Ω_+ has more ν_1 character, whereas in γ-Ca_2SiO_4, Ω_- has more ν_1 character, i.e., there is a crossover behavior. Piriou and McMillan (1983) used a model of two coupled harmonic oscillators to *correlate* the decrease in the frequencies with the crossover behavior in the mixing. They started with three simple harmonic oscillators whose natural frequencies are ω_3, ω_2, and ω_1 and whose characters are ν_3, ν_3, and ν_1, respectively. The ω_2 and ω_1 modes were assumed to be coupled with a coupling parameter β. Because of coupling, the eigen-frequencies are Ω_+ and Ω_-, where

$$\Omega_{\pm}^2 = \frac{\omega_1^2 + \omega_2^2}{2} \pm \left[\left(\frac{\omega_1^2 - \omega_2^2}{2}\right)^2 + \beta^4\right]^{1/2}. \quad (4)$$

[There is a typographical error in Eq. 1 of Piriou and McMillan (1983).] The amount of ν_1 and ν_3 characters in the Ω_+ and Ω_- mode depend on the relative values of ω_2 and ω_1 (see Piriou and McMillan, 1983, Eqs. 2a to 3b). If ω_2 is greater than ω_1, the lower mode has more ν_1 character. They *assumed* that these three frequencies decrease as a function of some parameter X; $\omega_1 = 858 - 24X$; $\omega_2 = 848 - 11.5X$; $\omega_3 = 993 - 43.5X$. The value of X for a given olivine was obtained using the assumed equation for ω_3. Some questions that one may ask are, (1) What is the physical meaning of the parameter X? and (2) Does the success of Piriou and McMillan's model in correlating the two observed trends imply that both trends have the same microscopic origin?

In view of our discussion in the section on Dependence of Vibrational Modes, the decrease of the high-frequency modes could, in principle, be caused by a decrease in the Si-O force constant, the intratetrahedral O-O force constant, or the intertetrahedral O-O force constant. Qualitatively, the parameter X represents a combination of these three interactions, but quantitatively, which interaction is dominant? First, we note that the decrease in ω_3 is much greater than that of Ω_+ and Ω_-. The ω_3 mode is basically Si-O_1 stretch, which has the shortest bond length. As the cation size increases, the SiO_4 tetrahedron becomes more regular, and the Si-O_1 bond increases. On the basis of our quantitative calculations, we find that the increase in the Si-O_1 distance alone cannot account for the large decrease in ω_3. The Si-O_1 distance is 1.634 Å in γ-Ca_2SiO_4 as compared to 1.615 Å in Mg_2SiO_4. We simulate the effect of Si-O_1 bond increase by decreasing the covalent term. As previously discussed, $d = 3.8$ for a Si-O distance of 1.615 Å and $d = 3.6$ for 1.634 Å. We find that ω_3 changes from 966 cm^{-1} to 945 cm^{-1} when the value of d changes from 3.8 to 3.6 (keeping everything else fixed). This is only a 21 cm^{-1} decrease as compared to the 40 cm^{-1} decrease observed. The intratetrahedral O-O distances increase somewhat (Piriou and McMillan, 1983, Fig. 5) but insignificantly. On the other hand, there is a significant change in the intertetrahedral O-O distances, about 10% from Mg_2SiO_4 to γ-Ca_2SiO_4. The dominant contribution to the O-O force constant comes from the Coulomb interaction; a 10% increase in distance causes a 30% decrease in the Coulomb force constant. A consistent explanation is that the decrease in ω_3 is caused not only by the increase in Si-O_1 distance but also by the increase in the intertetrahedral O-O distance, which decreases the intertetrahedral O-O Coulomb force constants. On the other hand, the Ω_+ and Ω_- modes involved mostly Si-O_3 and Si-O_2 stretching motion, respectively. Since the Si-O_3 and Si-O_2 distances change very little among the olivines (Piriou and McMillan, 1983, Fig. 5), the decrease in Ω_+ and Ω_- is caused mainly by the increase in the intertetrahedral O-O distance.

The mixing of ν_3 and ν_1 characters depends on the separation of the unperturbed ω_3 and ω_1 frequencies (controlled by the Si-O and intratetrahedral O-O force constants) and the strength of the mixing interaction (controlled by the intertetrahedral O-O force constant). As mentioned above, the Si-O_3 and Si-O_2 distances are relatively constant among the olivines; therefore, the dominant effect again comes from the variation in the intertetrahedral distances. For small cations where the intertetrahedral O-O distances are short, the intertetrahedral O-O Coulomb force constants are large, causing a large spreading of the ν_3- and ν_1-derived modes such that the ν_3-derived mode could be lower than the ν_1-derived modes (see also discussion in the section on Dependence of Vibration Modes and Fig. 4c). For large cations, the intertetrahedral O-O force constants are not large enough to cause a large spreading of the ν_3- and ν_1-derived modes (see Fig. 4b). The idea that large O-O Coulomb interaction can raise the ν_1-derived frequency above that of the ν_3-derived mode is also confirmed in our calculation by artificially increasing the charges on the oxygens. One prediction of our model is that applying pressure would increase the intertetrahedral O-O force constant and cause the lower mode to be more ν_3-like *provided* that the Si-O distances do not decrease significantly compared to the intertetrahedral O-O distances. One can observe this change in the ν_1 and ν_3 character with either an isotopic experiment or the relative intensities of the two A_g modes.

Summary

We have analyzed the microscopic interactions that are responsible for the distortion of the SiO_4 tetrahedron and

the systematic variation of the high-frequency modes of olivines. Our conclusions are summarized as follows:

1. The contraction of the SiO_4 tetrahedron is caused mainly by the Si-O covalent bonding.

2. The skewing of the tetrahedron is caused by forces on Si and O that come from the Si-Mg and O-Mg Coulomb interactions. In particular, the shortening of the Si-O_1 bond is caused by the Coulomb repulsion between the Mg ions at the base of the tetrahedron and the Si ion, which pushes the Si toward the O_1. The bending forces on O_2 and O_3 are caused by the combined effects of the covalent Si-O interaction and the O-Mg Coulomb attraction.

3. The SiO_4 tetrahedron becomes more regular as the cation size increases because the increase in the cation-Si distance causes a reduction in their Coulomb repulsion and thereby relaxes the shortening of the Si-O_1 bond and because the increase in the cation-oxygen distances reduces the distortion forces (the cation-oxygen Coulomb interaction) on the oxygens.

4. The systematic variation of three highest-frequency A_g modes, ω_3, Ω_+, and Ω_- (corresponding to the 824 cm^{-1}, 856 cm^{-1}, and 966 cm^{-1} modes in Mg_2SiO_4), in the olivines were examined. The decreases of the Ω_- and Ω_+ frequencies are caused mainly by the reduction in the intertetrahedral O-O Coulomb repulsion as the cation size increases. The decrease in the ω_3 frequency is caused by both the reduction in the intertetrahedral O-O Coulomb repulsion and the reduction in the Si-O covalent interaction due to the lengthening of the Si-O_1 bond.

5. The amount of ν_1-ν_3 mixing and the ordering of the ν_1- and ν_3-derived modes depend on the ratio (r_f) of the intratetrahedral O-O force constant to the Si-O force constant and the value of the intertetrahedral O-O force constant [intertetrahedral F(O-O)]. For the olivines, the ratio r_f is relatively constant because the average Si-O distance and intratetrahedral O-O distances are relatively constant. However, the intertetrahedral O-O distance varies by 10% as the cation size increases. We propose that the variation in the intertetrahedral O-O Coulomb interaction is responsible for the crossover behavior in the ν_1 and ν_3 mixing observed in the olivines.

Acknowledgments

We thank K. R. Rao and S. Ghose for providing us a preprint of their paper. The Cray computer time was provided by the San Diego Supercomputer Center. This work was supported by the National Science Foundation grant EAR-850891. We thank Glenn A. Waychunas and the two referees for their constructive comments. This is Hawaii Institute of Geophysics contribution no. 2141.

References cited

Baur, W.H. (1972) Computer-simulated crystal structures of observed and hypothetical Mg_2SiO_4 polymorphs of low and high density. American Mineralogist, 57, 704–731.

Birle, J.D., Gibbs, G.V., Moore, P.B., and Smith, J.V. (1968) Crystal structures of natural olivines. American Mineralogist, 53, 807–824.

Born, M., and Huang, K. (1954) Dynamical theory of crystal lattices. Oxford University Press, London.

Brown, G.E. (1980) Olivines and silicate spinels. In Mineralogical Society of America Reviews in Mineralogy, 5, 275–381.

Burns, G., and Glazer, A.M. (1978) Space groups for solid state scientists, p. 200–205. Academic Press, New York.

Bushing, W.R. (1981) WMIN, a computer program to model molecules and crystals in terms of potential energy functions. Oak Ridge National Laboratory, Oak Ridge.

Catti, M. (1981) The lattice energy of forsterite. Charge distribution and formation enthalpy of the SiO_4^{4+} ion. Physics and Chemistry of Minerals, 7, 20–25.

——— (1982) Atomic charges in $MgSiO_4$ (forsterite), fitted to thermoelastic and structural properties. Journal of Physics and Chemistry of Solids, 43, 1111–1118.

Hahn, T., Ed. (1983) International tables for crystallography, vol. A, p. 288, no. 62. D. Reidel, Dordrecht, Netherlands.

Handke, M. (1986) Vibrational spectra, force constants, and Si-O bond character in calcium silicate crystal structure. Applied Spectroscopy, 40, 871–877.

Hazen, R.M. (1976) Effects of temperature and pressure on the crystal structure of forsterite. American Mineralogist, 61, 1280–1293.

Iishi, K. (1978) Lattice dynamics of forsterite. American Mineralogist, 63, 1198–1208.

Kellermann, E.W. (1940) Theory of the vibrations of the sodium chloride lattice. Philosophical Transactions of the Royal Society of London, A238, 513–548.

Kieffer, S.W., and Navrotsky, A., Eds. (1985) Microscopic to macroscopic: Atomic environments to mineral thermodynamics. Mineralogical Society of America Reviews in Mineralogy, 14.

Maradudin, A.A. (1974) Elements of the theory of lattice dynamics. In G.K. Horton and A.A. Maradudin, Eds., Dynamical properties of solids, p. 1–82. North-Holland Publishing Company, Amsterdam.

Matsui, M., and Bushing, W.R. (1984) Computational modeling of the structure and elastic constants of the olivine and spinel forms of Mg_2SiO_4. Physics and Chemistry of Minerals, 11, 55–59.

Mclarnan, T.J., Hill, R.J., and Gibbs, G.V. (1979) A CNDO/2 molecular orbital study of shared tetrahedral edge conformations in olivine-type compounds. Australian Journal of Chemistry, 32, 949–959.

Miyamoto, M., and Takeda, H. (1980) An interpretation of the structures of mantle minerals at high pressure in terms of interatomic forces. Geochemical Journal, 14, 243–248.

Oehler, O., and Gunthard, Hs.H. (1969) Low-temperature infrared spectra between 1200 and 20 cm^{-1} and normal-coordinate analysis of silicates with olivine structure. Journal of Chemical Physics, 51, 4719–4728.

Paques-Ledent, M.Th., and Tarte, P. (1973) Vibrational studies of olivine-type compounds—I. The i.r. and Raman spectra of the isotopic species of Mg_2SiO_4. Spectrochimica Acta, 29A,1007–1016.

Parker, S.C. (1983) Prediction of mineral crystal structures. Solid State Ionics, 8, 179–186.

Pauling, L. (1960) The nature of the chemical bond (third edition), Chapters 7, 11, and 13. Cornell University Press, Ithaca, New York.

Piriou, B., and McMillan, P. (1983) The high-frequency vibrational spectra of vitreous and crystalline orthosilicates. American Mineralogist, 68, 426–443.

Price, G.D., and Parker, S.C. (1984) Computer simulations of the structural and physical properties of the olivine and spinel polymorphs of Mg_2SiO_4. Physics and Chemistry of Minerals, 10, 209–216.

Price, G.D., Parker, S.C., and Leslie, M. (1987) The lattice dynamics of forsterite. Mineralogical Magazine, 51, 157–70.

Rao, K.R., Chaplot, S.L., Choudhury, N., Ghose, S., and Price, D.L. (1987) Phonon density of states and specific heat of forsterite, Mg_2SiO_4. Science, 236, 64–65.

Rao, K.R., Chaplot, S.L., Choudhury, N., Ghose, S., Hastings, J.M., Corliss, L.M., and Price, D.L. (1988) Lattice dynamics and inelastic neutron scattering from forsterite, Mg_2SiO_4: Phonon dispersion relation, density of states and specific heat. Physics and Chemistry of Minerals, 16, 83–97.

Servoin, J.L., and Piriou, B. (1973) Infrared reflectivity and Raman scattering of Mg_2SiO_4 single crystal. Physica Status Solidi (b), 55, 677–686.

Manuscript received December 5, 1988
Manuscript accepted September 28, 1989